DALTON
FULL PAPER

# Dinuclear oxomolybdenum(V) complexes which show strong electrochemical interactions across bis-phenolate bridging ligands: a combined spectroelectrochemical and computational study

**Nicholas C. Harden, Elizabeth R. Humphrey, John C. Jeffery, Siu-Ming Lee, Massimo Marcaccio, Jon A. McCleverty,* Leigh H. Rees and Michael D. Ward ***

*School of Chemistry, University of Bristol, Cantock's Close, Bristol, UK BS8 1TS. E-mail: mike.ward@bristol.ac.uk; jon.mccleverty@bristol.ac.uk*

***Received 13th May 1999, Accepted 3rd June 1999***

A UV/VIS/NIR spectroelectrochemical study has been carried out on a series of dinuclear complexes of the type $[\{Mo(Tp^{Me,Me})(O)Cl\}_2\{\mu\text{-}OO\}]$, where 'OO' denotes a bis-phenolate bridging ligand and $Tp^{Me,Me}$ is tris(3,5-dimethylpyrazolyl)hydroborate. The bridging ligands are 1,4-$[O(C_6H_4)_nO]^{2-}$ ($n$ = 1 **1**, 2 **2**, 3 **3** or 4 **4**), 1,4-$[O(C_6H_3Me2)_2O]^{2-}$ **5**, 1,3-$[O(C_6H_4)O]^{2-}$ **6** and 1,4-$[OC_6H_4XC_6H_4O]^{2-}$ (X = $CH_2$ **7**, S **8** or $SO_2$ **9**). Thus **1**–**4** have oligophenylene spacers; in **5** the biphenyl bridge is twisted by the presence of the Me substituents, in contrast to **2** which has a normal biphenyl spacer; **6** has a *meta*-substituted phenylene bridge in contrast to the *para*-substituted analogue **1**; and **7**–**9** have single-atom spacers between the two phenyl rings. All complexes undergo two one-electron oxidations and two one-electron reductions, apart from **6** whose oxidation is irreversible. The effects of the different spacer groups on the electrochemical interactions in the complexes were examined by voltammetric determination of the redox splittings, the thioether spacer of **8** proving particularly effective at transmitting electronic interactions compared to the $SO_2$ bridge of **9**. UV/VIS/NIR Spectroelectrochemical studies on the mono- and di-oxidised complexes showed the presence of intense, low-energy phenolate→$Mo^{VI}$ charge-transfer bands; for example for $[\mathbf{4}]^{2+}$, $\lambda_{max}$ = 1033 nm ($\varepsilon$ = 50 000 $dm^3\ mol^{-1}\ cm^{-1}$). The assignments of these as LMCT transitions were confirmed by spectroelectrochemical studies on mononuclear model complexes $[Mo(Tp^{Me,Me})(O)Cl(OC_6H_4R)]$ (R = H **10** or OMe **11**) and by molecular orbital (ZINDO) calculations. Experimental and computational evidence indicate that the large separation between the two oxidations of **1**–**4** is ascribable in part to a near-planar bridging ligand conformation. The reduced forms of **1** and **6** were also examined by spectroelectrochemistry; whereas $[\mathbf{1}]^-$ [$Mo^{IV}Mo^V$ state] shows low-energy intervalence charge-transfer transitions across the *para*-substituted bridge, no such transitions are detectable across the *meta*-substituted bridge of $[\mathbf{6}]^-$.

## Introduction

We are interested in the study of electronic and magnetic metal–metal interactions across bridging ligands in polynuclear complexes,[1] with a view to the development of effective molecular wires,[2] an area of considerable current interest.[1–3] We recently prepared a series of dinuclear complexes $[\{Mo(Tp^{Me,Me})(O)Cl\}_2(\mu\text{-}OO)]$ [$Tp^{Me,Me}$ is tris(3,5-dimethylpyrazolyl)hydroborate] in which two oxomolybdenum(V) fragments are linked to the termini of various bis-phenolate bridging ligands ('OO') which were chosen to allow the systematic study of the effects of length, conformation, and substitution pattern of the bridging ligand on the magnetic and electrochemical interactions between the paramagnetic and redox-active termini (see complexes **1**–**6**).

The mononuclear complex building-block on which these dinuclear complexes are based is $[Mo(O)(Tp^{Me,Me})Cl(OPh)]$, which was first described by Enemark and co-workers[6] in 1987. Its most significant property for the purposes of this work is that it undergoes chemically reversible one-electron oxidation and reduction processes, which are formally $Mo^V$–$Mo^{VI}$ and $Mo^{IV}$–$Mo^V$ couples respectively. The dinuclear complexes are therefore expected to undergo two one-electron oxidations [to give the $Mo^V$–$Mo^{VI}$ and $Mo^{VI}_2$ states] and two one-electron reductions [to give the $Mo^V$–$Mo^{IV}$ and $Mo^{IV}_2$ states], and this was generally true with all redox processes for **2**–**5** being chemically fully reversible. For **1** only the first oxidation is reversible, and for **6** there are no reversible oxidations; however both complexes undergo the expected two reversible reductions. Although dinuclear complexes in which a strong electronic interaction between the metals allows access to a mixed-valence state are common,[2] those in which oxidation and reduction processes allow access to two different mixed-valence states are relatively rare.[7,8]

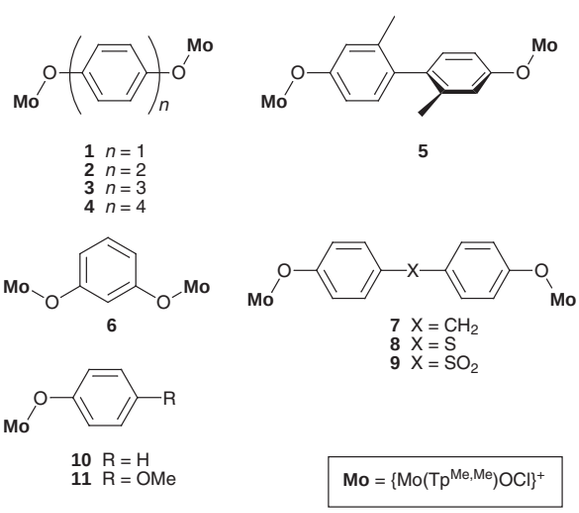


The work we describe here was prompted by an interesting feature of the electrochemical behaviour of these complexes: *viz.* for complexes **1**–**5**, in which there is an all-*para* linkage pattern across the bridging ligands, the redox potential separation between the two oxidations is much larger than the separation between the two reductions.[4] In **2** for example the two oxidations are 480 mV apart whereas the two reductions are almost

**Table 1** Characterisation data for the new complexes[a]

| Complex | Colour | Yield (%) | Elemental analytical data[b] (%) C | H | N | FAB-MS[c] *m/z* |
|---|---|---|---|---|---|---|
| **7** | Purple | 38 | 48.2 (47.5) | 5.0 (5.0) | 15.2 (15.5) | 1089 |
| **8** | Black | 31 | 44.9 (45.6) | 4.8 (4.7) | 14.8 (15.2) | 1107 |
| **8a** | Black | 38 | 48.7 (49.0) | 4.9 (4.7) | 12.6 (12.7) | 663 |
| **9** | Red | 23 | 44.8 (44.4) | 4.5 (4.6) | 14.5 (14.8) | 1138 |
| **9a** | Red | 27 | 46.1 (46.7) | 4.4 (4.5) | 11.8 (12.1) | 695 |
| **11** | Blue | 64 | 46.6 (46.4) | 5.1 (5.1) | 14.3 (14.8) | 569 |

[a] The IR spectra of all complexes (as KBr discs) showed $\nu_{B-H}$ in the range 2540–2560 $cm^{-1}$ and $\nu_{Mo=O}$ in the range 945–955 $cm^{-1}$. [b] Calculated values in parentheses. [c] Matrix: 3-nitrobenzyl alcohol.

coincident and cannot be resolved by cyclic or square-wave voltammetry. Thus the oxidised $Mo^{V}$–$Mo^{VI}$ mixed-valence states are much more stable with respect to disproportionation than are the reduced $Mo^{V}$–$Mo^{IV}$ mixed-valence states, and the extent of electronic delocalisation across the bridging ligand is substantially different in the two different mixed-valence states. This suggested to us that whereas the reductions are metal-localised and the interactions between them over these distances are therefore weak, the two oxidations could have some ligand-centred character, such that the doubly oxidised form could be expressed either as $Mo^{VI}$–$L^{2-}$–$Mo^{VI}$ (metal-based oxidations) or $Mo^{V}$–L–$Mo^{V}$ (ligand-based oxidations, to give a bridging quinone); see Scheme 1. A contribution from the


**Scheme 1** Extreme canonical forms of the doubly oxidised complexes: metal-centred oxidations to give two molybdenum(VI) centres (left), or ligand-centred oxidations to give a bridging quinone (right).

ligand-oxidised form would account for the strong electrochemical interaction between the two $Mo^{V}$–$Mo^{VI}$ couples because the positive charges would be much closer together, and this is also consistent with the ability of *para*-substituted dihydroxypolyphenyls to give quinones on oxidation.[9–12] We[13–16] and others[17] have recently described examples of ligand-centred redox processes involving the formation of bridging quinone-type ligands; spectroelectrochemical studies were generally essential to ascertain the nature of the redox processes concerned. A spectroelectrochemical study of these complexes therefore appeared highly desirable.

In this paper we describe the results of a detailed electrochemical, spectroelectrochemical and computational study of a series of nine such dinuclear complexes with various bridging ligands, carried out in order to clarify the nature of their electrochemical processes. The results were dramatic, with the oxidised forms of the complexes showing very intense new electronic transitions in the near-infrared (NIR) region of the spectrum. In addition to the previously reported complexes **1**–**6** with oligophenylene bridges, we describe also the new dinuclear complexes **7**–**9** which were prepared in order to extend our understanding of the effects of different bridging groups on metal–metal electronic interactions. Complex **7** contains a saturated $CH_2$ spacer between the two phenolate termini, and **8** and **9** contain respectively thioether (S) or sulfone ($SO_2$) spacers. The presence of single-atom spacers of this type will disrupt both the planarity and delocalisation across the bridging ligand, and makes it impossible for the bridging ligands to form a quinonoidal structure on oxidation; comparison of the electrochemical and spectroelectrochemical properties of these complexes with their fully conjugated analogues is therefore of interest. The crystal structures of dinuclear **8** and its mononuclear analogue **8a** are included. Two mononuclear complexes $[Mo(Tp^{Me,Me})(O)Cl(OC_6H_4R)]$ (R = H **10**, OMe **11**) were also examined, to assist with interpretation of the spectra of their dinuclear counterparts **1**–**9**.

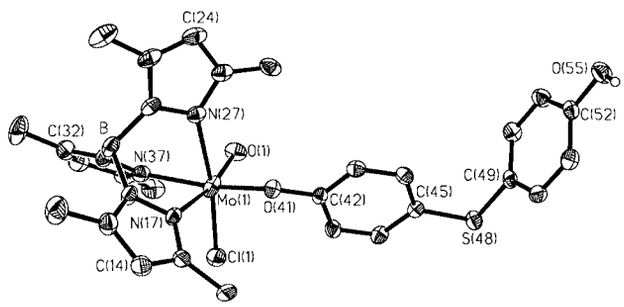


**Fig. 1** Crystal structure of complex **8a**.

In addition, we have performed molecular orbital calculations on some of the complexes to resolve the above-mentioned question of ligand-centred or metal-centred oxidation, and consequently assignment of the strong NIR transitions that occur in the mono- and di-oxidised forms of these complexes.

## Results and discussion

### (i) Syntheses of new complexes 7–9 and the crystal structures of 8 and 8a

The new complexes were all prepared in the same general way as the previously reported **1**–**6**, by reaction of the appropriate bis-phenol bridging ligands with an excess of $[Mo(Tp^{Me,Me})(O)Cl_2]$ in toluene at reflux in the presence of $Et_3N$.[4] The bis-phenols used for **7**–**9** are all commercially available. In every case the dinuclear complex was the main product and the first to elute from a silica column; traces of the mononuclear analogues, in which one phenol site is co-ordinated and the other pendant, are more polar and eluted after the dinuclear complexes. These were generally present in small amounts and the only ones isolated and characterised were **8a** and **9a**, the mononuclear counterparts of **8** and **9**. Characterisation data for all new complexes are collected in Table 1.

The crystal structures of **8a** and **8** are shown in Figs. 1 and 2 respectively and are fairly self-explanatory; see Tables 2 and 3 for the bond lengths and angles. In each case the co-ordination geometries and metrical parameters of the metal centres are unremarkable and comparable to those of the previously determined structures in this series.[4,5,18] The Mo–O and Mo–Cl distances in both structures are (as usual) rendered rather inaccurate by the occurrence of disorder between the O and Cl atoms; only the major component of the disorder is shown in the Figures. The C–S–C angles in the thiodiphenol ligands are 102.78(14) and 103.4(2)° for **8a** and **8** respectively, which are statistically identical. This shows that there is no significant steric interaction between the two metal complex units in dinuclear **8** which, if it occurred, would be expected to increase

the C–S–C angle. The two phenyl rings in the ligands are approaching orthogonality in each case, with angles between their mean planes of 82.9° in **8a** and 77.4° in **8**. This implies that it is not possible in this conformation for a π-symmetry orbital (d or p) on the S atom to interact with both phenyl π systems simultaneously; this point is significant for discussion of the electrochemical data (below).

### (ii) Electrochemical studies on the new dinuclear complexes 7–9

Electrochemical data are summarised in Table 4; the data for **1**–**6** are included for comparison with the new complexes. The mononuclear complexes **8a** and **9a** show the expected chemically reversible one-electron $Mo^{V}$–$Mo^{VI}$ and $Mo^{IV}$–$Mo^{V}$ couples. Comparison with the parent mononuclear complex [Mo($Tp^{Me,Me}$)(O)Cl(OPh)] **10**[4] shows how the $Mo^{V}$–$Mo^{VI}$ redox potentials reflect the electron-donating effect of the thioether substituent (shift towards more negative potentials because the electron-rich metal is easier to oxidise and harder to reduce) and the electron withdrawing effect of the sulfone (shift towards more positive potentials because the electron-poor metal centre is harder to oxidise and easier to reduce). The $Mo^{IV}$–$Mo^{V}$ redox potentials in contrast appear to be much less sensitive to the effects of substituents on the phenolate ligand, consistent with the poor delocalisation of the negative charges of the mixed-valence states $[\mathbf{1}]^{-}$–$[\mathbf{6}]^{-}$ across the bridging ligands that is apparent from electrochemical data.

The dinuclear complex **7** shows the same general behaviour as that of **1**–**4**,[4] with two $Mo^{V}$–$Mo^{VI}$ couples separated by 120 mV but two $Mo^{IV}$–$Mo^{V}$ couples essentially coincident giving a single double-intensity wave in the voltammogram. Compared to complex **2** (two phenylene spacers) where this redox separation is 480 mV, the greatly reduced redox separation for **7** is clearly ascribable to the saturated $CH_2$ spacer. This breaks the conjugation across the bridging ligand, and thereby prevents delocalisation of charge beyond each individual phenyl ring

**Table 2** Selected bond lengths (Å) and angles (°) for complex **8a**[a]

| | | | |
|---|---|---|---|
| Mo(1)–O(1′) | 1.720(6) | Mo(1)–N(27) | 2.268(3) |
| Mo(1)–O(1) | 1.847(10) | Mo(1)–N(17) | 2.221(3) |
| Mo(1)–O(41) | 1.962(2) | Mo(1)–Cl(1) | 2.242(2) |
| Mo(1)–N(37) | 2.168(3) | Mo(1)–Cl(1′) | 2.214(4) |
| | | | |
| O(1′)–Mo(1)–O(41) | 101.7(3) | O(1)–Mo(1)–Cl(1) | 98.9(5) |
| O(1)–Mo(1)–O(41) | 96.2(5) | O(41)–Mo(1)–Cl(1) | 99.04(9) |
| O(1′)–Mo(1)–N(37) | 89.7(3) | N(37)–Mo(1)–Cl(1) | 93.60(10) |
| O(1)–Mo(1)–N(37) | 90.4(5) | N(17)–Mo(1)–Cl(1) | 92.79(10) |
| O(41)–Mo(1)–N(37) | 164.68(9) | O(1′)–Mo(1)–N(27) | 163.8(3) |
| O(1′)–Mo(1)–Cl(1′) | 101.9(3) | O(1)–Mo(1)–N(27) | 86.6(5) |
| O(41)–Mo(1)–Cl(1′) | 93.4(2) | O(41)–Mo(1)–N(27) | 85.88(9) |
| N(37)–Mo(1)–Cl(1′) | 94.3(2) | N(37)–Mo(1)–N(27) | 80.68(10) |
| O(1′)–Mo(1)–N(17) | 84.8(3) | Cl(1′)–Mo(1)–N(27) | 91.8(2) |
| O(1)–Mo(1)–N(17) | 167.5(4) | N(17)–Mo(1)–N(27) | 81.35(9) |
| O(41)–Mo(1)–N(17) | 86.41(9) | Cl(1)–Mo(1)–N(27) | 172.14(10) |
| N(37)–Mo(1)–N(17) | 84.35(10) | Cl(1′)–Mo(1)–N(17) | 173.1(2) |

[a] The bond distances and angles involving the disordered atoms O(1)/O(1′) and Cl(1)/Cl(1′) should be treated with caution as they are likely to be considerably less reliable than the others.

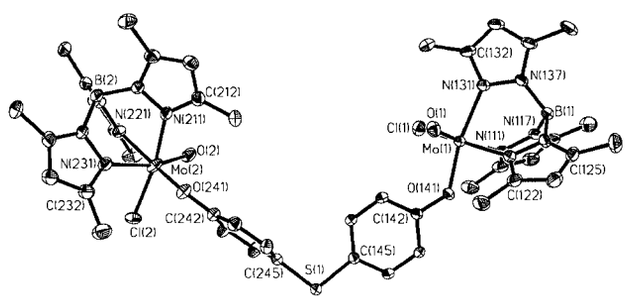


**Fig. 2** Crystal structure of complex **8**.

**Table 3** Selected bond lengths (Å) and angles (°) for complex **8**[a]

| | | | |
|---|---|---|---|
| Mo(1)–O(1′) | 1.810(14) | Mo(2)–O(2) | 1.716(10) |
| Mo(1)–O(1) | 1.83(2) | Mo(2)–O(2′) | 1.825(13) |
| Mo(1)–O(141) | 1.945(3) | Mo(2)–O(241) | 1.947(3) |
| Mo(1)–Cl(1) | 2.165(6) | Mo(2)–N(221) | 2.180(3) |
| Mo(1)–N(131) | 2.187(3) | Mo(2)–N(211) | 2.209(3) |
| Mo(1)–N(111) | 2.220(3) | Mo(2)–Cl(2′) | 2.211(5) |
| Mo(1)–Cl(1′) | 2.242(5) | Mo(2)–N(231) | 2.250(3) |
| Mo(1)–N(121) | 2.254(3) | Mo(2)–Cl(2) | 2.273(4) |
| | | | |
| O(1′)–Mo(1)–O(141) | 100.1(5) | O(2)–Mo(2)–O(241) | 98.9(4) |
| O(1)–Mo(1)–O(141) | 98.5(6) | O(2′)–Mo(2)–O(241) | 98.7(5) |
| O(1)–Mo(1)–Cl(1) | 101.2(6) | O(2)–Mo(2)–N(221) | 88.2(4) |
| O(141)–Mo(1)–Cl(1) | 93.1(2) | O(2′)–Mo(2)–N(221) | 88.6(5) |
| O(1′)–Mo(1)–N(131) | 86.9(5) | O(241)–Mo(2)–N(221) | 168.25(12) |
| O(1)–Mo(1)–N(131) | 88.2(6) | O(2)–Mo(2)–N(211) | 88.8(3) |
| O(141)–Mo(1)–N(131) | 168.55(12) | O(2′)–Mo(2)–N(211) | 165.1(5) |
| Cl(1)–Mo(1)–N(131) | 94.6(2) | O(241)–Mo(2)–N(211) | 86.78(12) |
| O(1′)–Mo(1)–N(111) | 88.1(5) | N(221)–Mo(2)–N(211) | 84.01(12) |
| O(1)–Mo(1)–N(111) | 163.4(6) | O(2′)–Mo(2)–Cl(2′) | 99.5(5) |
| O(141)–Mo(1)–N(111) | 88.16(12) | O(241)–Mo(2)–Cl(2′) | 94.4(2) |
| Cl(1)–Mo(1)–N(111) | 93.6(2) | N(221)–Mo(2)–Cl(2′) | 93.4(2) |
| N(131)–Mo(1)–N(111) | 83.01(12) | N(211)–Mo(2)–Cl(2′) | 93.8(2) |
| O(1′)–Mo(1)–Cl(1′) | 102.0(5) | O(2)–Mo(2)–N(231) | 165.5(3) |
| O(141)–Mo(1)–Cl(1′) | 94.8(2) | O(2′)–Mo(2)–N(231) | 87.4(5) |
| N(131)–Mo(1)–Cl(1′) | 92.6(2) | O(241)–Mo(2)–N(231) | 88.08(12) |
| N(111)–Mo(1)–Cl(1′) | 168.8(2) | N(221)–Mo(2)–N(231) | 83.01(13) |
| O(1′)–Mo(1)–N(121) | 164.8(4) | N(211)–Mo(2)–N(231) | 78.90(12) |
| O(1)–Mo(1)–N(121) | 86.3(6) | Cl(2′)–Mo(2)–N(231) | 172.1(2) |
| O(141)–Mo(1)–N(121) | 87.21(12) | O(2)–Mo(2)–Cl(2) | 102.8(3) |
| Cl(1)–Mo(1)–N(121) | 172.4(2) | O(241)–Mo(2)–Cl(2) | 92.56(14) |
| N(131)–Mo(1)–N(121) | 83.95(12) | N(221)–Mo(2)–Cl(2) | 94.98(14) |
| N(111)–Mo(1)–N(121) | 78.81(13) | N(211)–Mo(2)–Cl(2) | 168.33(14) |
| Cl(1′)–Mo(1)–N(121) | 90.5(2) | N(231)–Mo(2)–Cl(2) | 89.43(14) |

[a] The bond distances and angles involving the disordered atoms O(1)/O(1′) and Cl(1)/Cl(1′) should be treated with caution as they are likely to be considerably less reliable than the others.

**Table 4** Electrochemical data[a]

| Complex | $E$/V *vs.* Fc–Fc$^+$ | | |
|---|---|---|---|
| | $Mo^{IV}$–$Mo^{V}$ couple | $Mo^{V}$–$Mo^{VI}$ couple | $\Delta E_{1/2}$/mV |
| **1** | −1.19, −1.44 | +0.26, +1.25[c] | 990 |
| **2** | −1.13[b] | +0.44, +0.92 | 480 |
| **3** | −1.16[b] | +0.56, +0.74 | 180 |
| **4** | −1.16[b] | +0.61[b] | [d] |
| **5** | −1.21[b] | +0.55, +0.78 | 230 |
| **6** | −1.20, −1.40 | +0.58[c] | — |
| **7** | −1.23[b] | +0.60, +0.72 | 120 |
| **8** | −1.16[b] | +0.45, +0.88 | 430 |
| **8a** | −1.16 | +0.48 | — |
| **9** | −1.07[b] | +0.88, +0.96 | 80 |
| **9a** | −1.02 | +0.91 | — |
| **10** | −1.21 | +0.68 | — |
| **11** | −1.28 | +0.44 | — |

[a] All measurements made in $CH_2Cl_2$ containing 0.1–0.2 M $Bu_4NPF_6$ as base electrolyte using a Pt-bead working electrode. Data for complexes **1**–**6** are reproduced from ref. 4. [b] Two coincident one-electron couples. [c] Irreversible process. [d] Redox separation is too small to measure.

which becomes effectively electronically isolated from its neighbour. A similar effect with this ligand has been observed before.[19]

For complex **8**, where the $CH_2$ spacer is replaced by S, the separation between the two $Mo^{V}$–$Mo^{VI}$ couples has increased to 430 mV, and is therefore almost restored to the value observed for the fully conjugated complex **2** despite the increased length of the bridge and presence of a formally saturated, tetrahedral spacer [Fig. 3(*a*)]. The marked contrast with the behaviour of **7** shows that the thioether S atom of **8** is clearly playing a significant role in facilitating electronic delocalisation across the bridging ligand. Although the only other studies of metal–metal interactions across a diaryl thioether bridging ligand of this sort showed the interactions to be rather weak,[19,20] we note that a *di*sulfide bridge between two pyridyl rings has recently been shown to be very effective at transmitting electronic interactions, because of overlap of relatively extended π-symmetry (p or d) orbitals on the sulfur atoms with the π systems of the phenyl rings.[21] We suggest that a similar effect is operative in complex **8**; this would require a significant conformational change from that observed in the crystal structure, in which the two phenyl rings of the bridging ligand are nearly orthogonal. We note that for **8** the strong electronic interaction cannot be ascribed to formation of a quinone structure by ligand-centred oxidation (*cf.* Scheme 1).

For complex **9** the electron-withdrawing sulfone group in the bridging ligand shifts the redox processes towards more positive potentials compared to those of **7** and **8**, but the main difference between **9** and **8** is that the redox splitting between the $Mo^{V}$–$Mo^{VI}$ couples has decreased from 430 mV in **8** to just 80 mV in **9**, even less than the coupling across the $CH_2$ spacer of **7**, despite the through-bond separation between the metal centres being unchanged [Fig. 3(*b*)]. Oxidation of the sulfur atom to the +6 oxidation state will result in considerable contraction of its orbitals, such that any overlap with the π system of the phenyl rings will be reduced. In addition, whereas a p(π) orbital on the thioether S atom in **8** might be available to interact with the phenyl π systems if the S atom were $sp^2$ hybridised, the necessary $sp^3$ hybridisation of the tetrahedral sulfone S atom in **9** makes this impossible. Whichever explanation is more appropriate it is clear that oxidation of the thioether to a sulfone has almost completely removed its ability to act as conduit for π-electron delocalisation, which constitutes an interesting (albeit irreversible) switching effect. A similar effect has been observed before, but more weakly: the effect is much more dramatic with complex **9**.[19]

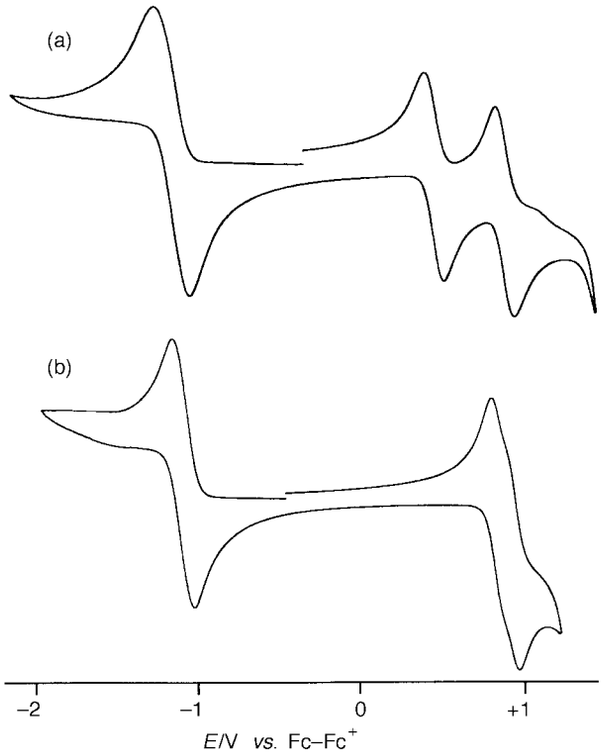


**Fig. 3** Cyclic voltammograms of complex **8** (*a*) and **9** (*b*).

### (iii) Spectroelectrochemical studies on mononuclear complexes 10 and 11

Before studying the spectroelectrochemical properties of the dinuclear complexes we first need to understand the electronic spectra of the mononuclear components in their accessible oxidation states (+4, +5, +6). Accordingly we performed spectroelectrochemical studies on the mononuclear oxomolybdenum(V) complexes **10** and **11** (the studies on **10** were briefly reported earlier).[14] Both complexes undergo chemically reversible one-electron oxidation and reduction processes, giving formally molybdenum(VI) and -(IV) species respectively. Their electrochemical properties are summarised in Table 4, and the results of the UV/VIS/NIR spectroelectrochemical study are in Table 5.

In the electronic spectrum of complex **10** the lowest-energy feature at 520 nm we ascribed to a phenolate→$Mo^{V}$ LMCT process; the higher-energy transitions at 340 and 266 nm are probably Cl(π)→Mo($d_{xy}$) LMCT and ligand-centred π ⟶ π* processes respectively.[4] On one-electron oxidation, formally a metal-centred process generating $Mo^{VI}$, the phenolate-to-$Mo^{V}$ LMCT band is replaced by two more intense bands at 475 and 681 nm. Since metal-centred oxidation will both lower the energy of the metal d(π) orbitals and increase their electron-accepting ability, we might expect the phenolate→Mo LMCT at 520 nm to become red-shifted and to increase in intensity. On this basis the 681 nm transition is assigned to a phenolate→$Mo^{VI}$ LMCT transition. The additional new transition at 475 nm is also likely to be an LMCT band of some sort. We note that the three d(π) orbitals are non-degenerate, with the d(*xy*) orbital lying below d(*xz*) and d(*yz*) (which are raised in energy by interaction with the π-donor oxo-ligand);[4] two phenolate→d(π) LMCT transitions might therefore be expected.

The behaviour of complex **11** is similar to that of **10**, with the effect of the substituents on the phenolate being clear: the phenolate→$Mo^{V}$ LMCT is red-shifted to 593 nm in **11**, because the filled ligand-based orbitals are raised nearer to the metal orbitals by the electron-donor substituent. On oxidation to the molybdenum(VI) state these are again replaced by two intense

**Table 5** Summary of spectroelectrochemical data ($CH_2Cl_2$, 243 K)

| Complex | $\lambda_{max}$/nm ($10^{-3}$ $\varepsilon$/dm$^3$ mol$^{-1}$ cm$^{-1}$) | | | | |
|---|---|---|---|---|---|
| **1** | 660 (5.1)[a] | 397 (7.8) | 266 (15) | | |
| $[\mathbf{1}]^+$ | 817 (12)[b] | 700 (sh) | 566 (18)[b] | 307 (11) | |
| $[\mathbf{1}]^-$ | ≈1700 (sh)[c] | 1127 (2.1)[c] | 746 (2.7)[a] | 430 (4.3) | 290 (sh) |
| $[\mathbf{1}]^{2-}$ | 800 (0.3)[d] | 383 (7.7) | 300 (7.7) | | |
| **2** | 614 (6.7)[a] | 389 (14.5) | 272 (33.1) | | |
| $[\mathbf{2}]^+$ | 1096 (50)[b] | 643 (15) | 475 (10) | 311 (14) | |
| $[\mathbf{2}]^{2+}$ | 1017 (48)[b] | 599 (11) | 475 (12) | 353 (15) | |
| **3** | 592 (5.4)[a] | 373 (16) | 297 (31) | | |
| $[\mathbf{3}]^+$ | 1131 (25)[b] | 600 (9.8) | 374 (13) | 273 (16) | |
| $[\mathbf{3}]^{2+}$ | 1015 (62)[b] | 567 (sh) | 357 (17) | | |
| **4** | 586 (5.2)[a] | 380 (sh) | 311 (33) | | |
| $[\mathbf{4}]^+$ | 1047 (24)[b] | 562 (7.7) | 310 (20) | 277 (21) | |
| $[\mathbf{4}]^{2+}$ | 1033 (50)[b] | 548 (9.0) | 302 (17) | 283 (17) | |
| **5** | 570 (5.9)[a] | 364 (14) | 262 (sh) | | |
| $[\mathbf{5}]^+$ | 1245 (19)[b] | 580 (10) | | | |
| $[\mathbf{5}]^{2+}$ | 832 (32)[b] | 479 (11) | 357 (14) | | |
| **6** | 544 (3.3)[a] | 352 (10) | 266 (19) | | |
| $[\mathbf{6}]^-$ | 627 (1.5)[a] | 360 (6.8) | 280 (15) | | |
| $[\mathbf{6}]^{2-}$ | 860 (0.1)[d] | 430 (sh) | 372 (4.5) | 286 (10) | |
| **7** | 533 (4.8)[a] | 358 (13) | 264 (23) | | |
| $[\mathbf{7}]^+$ | 733 (20)[b] | 595 (12) | 520 (sh) | 351 (14) | 265 (19) |
| $[\mathbf{7}]^{2+}$ | 771 (37)[b] | 595 (22) | 515 (13) | 354 (16) | 260 (17) |
| **8** | 578 (4.2)[a] | 361 (12) | 260 (29) | | |
| $[\mathbf{8}]^+$ | ≈1200 (sh)[b] | 900 (8.2)[b] | 595 (7.4) | 360 (sh) | 260 (24) |
| $[\mathbf{8}]^{2+}$ | ≈1200 (sh)[b] | 900 (15)[b] | 600 (10) | ≈300 (sh) | |
| **9** | 497 (5.2)[a] | 348 (19) | 267 (30) | | |
| $[\mathbf{9}]^+$ | 695 (12)[b] | 485 (9.2) | 348 (18) | 260 (21) | |
| $[\mathbf{9}]^{2+}$ | 699 (24)[b] | 486 (sh) | 350 (18) | | |
| **8a** | 570 (2.3)[a] | 362 (6.8) | 260 (19) | | |
| **9a** | 489 (2.5)[a] | 325 (sh) | 263 (21) | | |
| **10** | 520 (1.8)[a] | 340 (6.2) | 266 (9.8) | | |
| $[\mathbf{10}]^+$ | 681 (13)[b] | 475 (5.4)[b] | 359 (6.8) | | |
| **11** | 593 (3.1)[a] | 369 (6.3) | 268 (11) | | |
| $[\mathbf{11}]^+$ | 724 (9.6)[b] | 554 (7.0)[b] | 352 (8.0) | 272 (10) | |
| $[\mathbf{11}]^-$ | 830 (0.5)[d] | 369 (3.2) | 294 (11) | | |

[a] Phenolate→$Mo^V$ LMCT. [b] Phenolate→$Mo^{VI}$ LMCT. [c] $Mo^{IV}$→$Mo^V$ IVCT. [d] Molybdenum(IV) d–d transition.

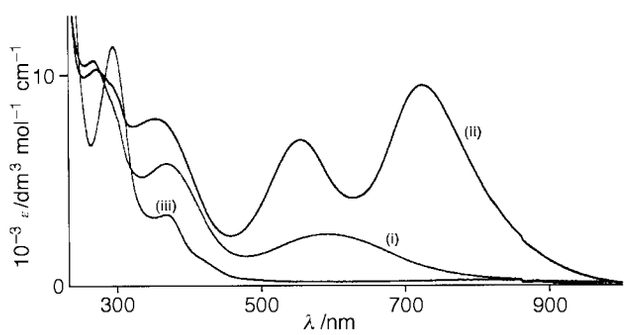


**Fig. 4** Electronic spectra of complex **11** (i), $[\mathbf{11}]^+$ (ii) and $[\mathbf{11}]^-$ (iii).

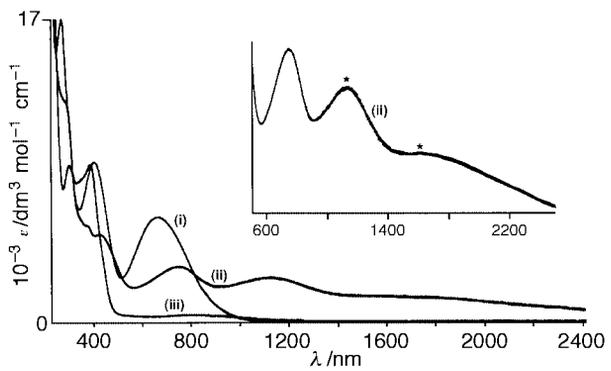


**Fig. 5** Electronic spectra of complex **1** (i), $[\mathbf{1}]^-$ (ii) and $[\mathbf{1}]^{2-}$ (iii). Inset is an expansion of the near-IR region of the spectrum of $[\mathbf{1}]^-$ with the IVCT bands labelled *.

new transitions (Fig. 4). The fact that *both* new transitions are red-shifted compared to the two analogous transitions of $[\mathbf{10}]^+$, an obvious effect arising from the electron-donating substituents on the phenolate ligand, confirms that both of these transitions have phenolate→$Mo^{VI}$ LMCT character (see also the ZINDO calculations below).

On reduction of these mononuclear complexes to the molybdenum(IV) state the phenolate→$Mo^V$ LMCT band completely disappears such that the complexes are essentially transparent above about 500 nm (Fig. 4). The only exception to this is a weak d–d transition at about 800 nm, arising from a transition between the filled d(*xy*) level and the empty d(*xz*) and d(*yz*) levels. Such low-energy d–d transitions have been observed for complexes of $Ru^{III}$ in which a distorted pseudo-octahedral geometry splits the '$t_{2g}$' orbital set.[22]

### (iv) Reductions of dinuclear complexes 1 and 6

The dinuclear complexes **1** and **6** contain two {$Mo^V(Tp^{Me,Me})$-(O)Cl} fragments, linked by the deprotonated dianion of 1,4-dihydroxybenzene and 1,3-dihydroxybenzene, respectively: accordingly they differ only in the substitution pattern of the bridging ligand, and this has been shown to result in significant differences between their electrochemical and magnetic properties.[4,5]

The electronic spectra of complexes **1**, $[\mathbf{1}]^-$ and $[\mathbf{1}]^{2-}$ are shown in Fig. 5. In the $Mo^V_2$ state the spectrum of **1** shows the expected LMCT transition at 660 nm arising from the bridging ligand, directly analogous to the phenolate→$Mo^V$ LMCT bands of mononuclear **7**–**9**. The expected higher-energy LMCT and $\pi \longrightarrow \pi^*$ transitions are also apparent, and overall there is an obvious correspondence between the spectra of dinuclear **1** and mononuclear **10**. On one-electron reduction to the $Mo^V$-$Mo^{IV}$ form the 660 nm LMCT transition approximately halves in intensity and is red-shifted to 746 nm. This intensity reduction is consistent with the presence of one molybdenum(V)

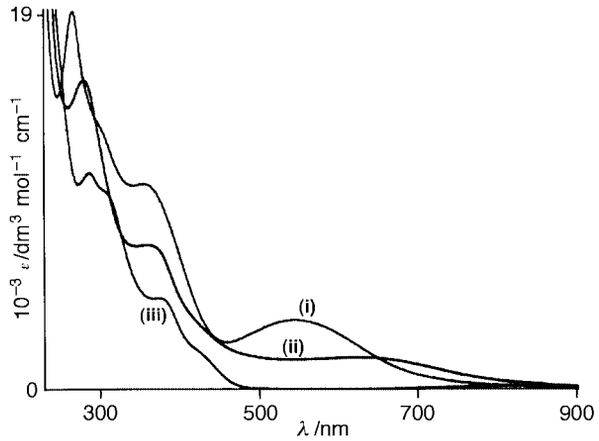


**Fig. 6** Electronic spectra of complex **6** (i), $[\mathbf{6}]^-$ (ii) and $[\mathbf{6}]^{2-}$ (iii).

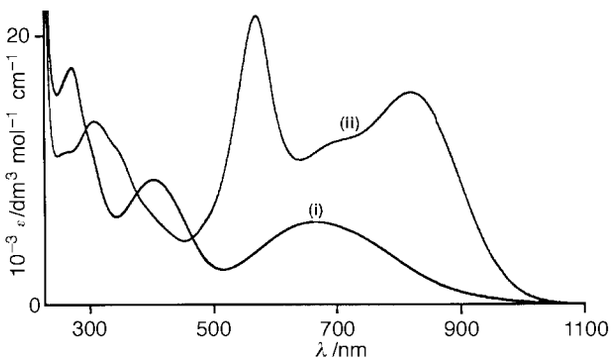


**Fig. 7** Electronic spectra of complex **1** (i) and $[\mathbf{1}]^+$ (ii).

centre in the complex instead of two, and the red-shift of this LMCT band at the remaining molybdenum(v) site occurs because reduction of the other metal to $Mo^{IV}$ will raise the orbitals of the bridging ligand in energy. In addition, new transitions are apparent at 1127 and *ca.* 1700 nm, the latter of which is very broad and extends completely across the NIR region out to 3000 nm. From our studies on **10** and **11** we know that mononuclear molybdenum(IV) and molybdenum(V) centres of this type have no transitions in this region, so we ascribe these to $Mo^{IV}\rightarrow Mo^{V}$ intervalence charge-transfer (IVCT) bands. This assignment is confirmed by the fact that they completely disappear following the second reduction to the $Mo^{IV}_2$ state in $[\mathbf{1}]^{2-}$. The observation of a transition ascribable to a localised molybdenum(v) site in the mixed valence state (at 746 nm) means that $[\mathbf{1}]^-$ could be classified as a class II mixed valence species, although the presence of the IVCT bands shows that there is a significant interaction between the metal centres. The presence of two identifiable IVCT bands may be related to the substantial splitting of the d($\pi$) orbital set on each metal, such that the electron which originates from a filled d(*xy*) orbital on the molybdenum(IV) centre could transfer either to the half-empty d(*xy*) level or the completely empty d(*xz*)/d(*yz*) level on the molybdenum(v) centre.

Comparison with the spectra of complex **6**, $[\mathbf{6}]^-$ and $[\mathbf{6}]^{2-}$ (Fig. 6) is interesting as the effect of the substitution pattern on the bridging ligand becomes apparent. In the spectrum of **6** the lowest-energy LMCT transition (bridging ligand to metal) is at 544 nm; this is similar to the position of the phenolate$\rightarrow Mo^{V}$ LMCT in **10**, because the *meta*-substitution pattern of the bridging ligand results in each donor atom of the bridging ligand behaving more like an electronically isolated phenolate than was the case for **1**, where this transition is at 660 nm. Reduction to $[\mathbf{6}]^-$ [the mixed-valence $Mo^{V}Mo^{IV}$ state] again results in an approximate halving of the intensity of this LMCT band coupled to a red-shift to 627 nm, consistent (as for $[\mathbf{1}]^-$) with the presence of localised molybdenum(v) and -(IV) centres.

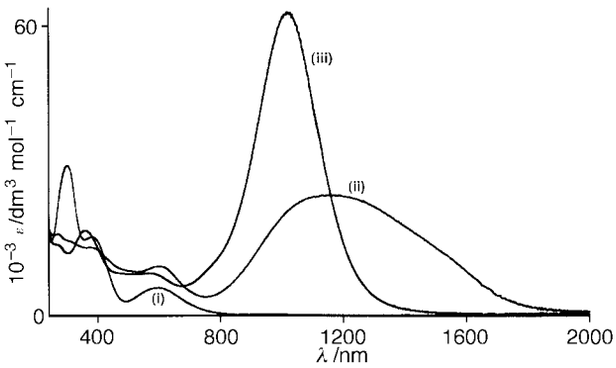


**Fig. 8** Electronic spectra of complex **3** (i), $[\mathbf{3}]^+$ (ii) and $[\mathbf{3}]^{2+}$ (iii).

However, in this case the additional low-energy IVCT bands, which were such a striking feature of the spectrum of $[\mathbf{1}]^-$, are completely absent, suggesting that the *meta*-substitution pattern has substantially attenuated the metal–metal electronic coupling. The 200 mV separation between the two $Mo^{V}$–$Mo^{IV}$ couples of **6** does suggest that the electronic interaction between the metal centres is still significant.[2] However it is possible that this redox splitting is largely ascribable to a through-space Coulombic effect because the metals are so close together,[4] such that there is little contribution to the stability of the mixed-valence state arising from delocalisation across the bridging ligand: this would account for the lack of IVCT bands. It has been pointed out before that dinuclear complexes with strong electrochemical interactions (*i.e.* large $\Delta E_{1/2}$ values) can still have very weak IVCT features in their electronic spectra if the relative orientations of the metal fragments and the bridging ligand preclude efficient orbital overlap.[15] The most appropriate description of $[\mathbf{6}]^-$ is therefore (at most) weakly coupled class II, in obvious contrast to $[\mathbf{1}]^-$. This dependence of the nature of the mixed-valence state on the substitution pattern of the bridging ligand has been noted before, in dinuclear $Mo^{II}Mo^{I}$ complexes with *ortho*-, *meta*- and *para*-$[HNC_6H_4NH]^{2-}$ as bridging ligands.[16]

### (v) Oxidations of the dinuclear complexes 1–5 and 7–9

Although complex **1** undergoes two oxidation processes with a very large separation of 990 mV between them, only the first is chemically reversible; the spectrum of $[\mathbf{1}]^+$ (together with that of **1**) is in Fig. 7. Attempts to study the spectral behaviour of $[\mathbf{1}]^{2+}$ proved, as expected, unsuccessful because the irreversibility of this process clearly results in decomposition of the complex. Mono-oxidation of the complex has resulted in replacement of the lowest-energy MLCT transition of **1** at 660 nm by two more intense new transitions, one at lower energy (817 nm) and one at higher energy (566 nm). This behaviour is similar to that of the mononuclear complexes **10** and **11** (compare with the spectrum of $[\mathbf{11}]^+$ in Fig. 4), and suggests that the first oxidation of **1** is in fact metal-centred to give a $Mo^{V}$–$Mo^{VI}$ species. Whether this is class II or class III is not obvious: the large separation between the oxidation potentials suggests class III behaviour, but there is no evidence for a new IVCT transition in the near-IR region out to 3000 nm.

Complexes **2**–**4** behave similarly to one another on oxidation. The first oxidation results in the appearance of an intense new transition in the near-IR region which, after the second oxidation, moves to slightly higher energy (Table 5, Fig. 8). For the fully oxidised complexes $[\mathbf{2}]^{2+}$, $[\mathbf{3}]^{2+}$ and $[\mathbf{4}]^{2+}$ the absorption maxima are at almost identical positions (1017, 1015 and 1033 nm respectively) and have very high intensities (*ca.* 50 000 dm$^3$ mol$^{-1}$ cm$^{-1}$). Complex **5** behaves generally similarly, although the effect of the methyl substituents on the bridging ligand, which force it to adopt a twisted conformation with the two halves near-orthogonal, is clear by comparison with the spectra of **2**. In particular the principal low-energy transition in the

spectrum of the fully oxidised form $[\mathbf{5}]^{2+}$ is at higher energy than that of $[\mathbf{2}]^{2+}$ (832 nm, compared to 1017 nm), consistent with the fact that decoupling the π systems of the two phenyl rings should make each terminus behave more like an electronically isolated phenolate (*cf.* the spectrum of $[\mathbf{10}]^{+}$, $\lambda_{max}$ = 681 nm). The natures of these electronic transitions for complexes **1**–**5** will be discussed later. Complex **6** undergoes no reversible oxidations.

Oxidation of complex **7** to $[\mathbf{7}]^{+}$ results in a strong transition appearing at 733 nm, which is not very different from that observed for the mononuclear phenolate complex $[\mathbf{10}]^{+}$ (although more intense). For this reason, and because of the obvious fact that ligand-centred oxidations to give a quinonoidal structure are not possible for **7**, we ascribe this to a simple phenolate→Mo LMCT transition as seen for the mononuclear complexes. On further oxidation to $[\mathbf{7}]^{2+}$ this transition approximately doubles in intensity whilst only changing in energy slightly, consistent with sequential oxidation of two equivalent but electronically near-independent chromophores giving first one and then two equivalent, localised phenolate→$Mo^{VI}$ LMCT transitions. Similar behaviour was observed during oxidation of **9** to $[\mathbf{9}]^{+}$ and then $[\mathbf{9}]^{2+}$. The contrast of these with the behaviour of the more strongly coupled complexes **1**–**5**, in which (i) the LMCT transitions in the oxidised forms are in the near-IR region and (ii) the singly- and doubly-oxidised forms can give quite different spectra, is obvious. In $[\mathbf{8}]^{+}$ the LMCT transition is at lower energy than those of $[\mathbf{7}]^{+}$ and $[\mathbf{9}]^{+}$, and also has a marked low-energy shoulder at about 1200 nm; it appears that the strong electronic coupling between the metals that arises from participation of the thioether bridging group in delocalisation also results in the LMCT transition in the mixed-valence state being red-shifted. Further oxidation of $[\mathbf{8}]^{+}$ to $[\mathbf{8}]^{2+}$ results in no change in the position of this band but an approximate doubling in intensity. This behaviour is again consistent with the two LMCT bands behaving independently of one another, despite the strong redox separation between the $Mo^{V}$–$Mo^{VI}$ couples of this complex.

Reductions of representative complexes to the $Mo^{V}Mo^{IV}$ and finally the $Mo^{IV}_{2}$ states were uninteresting, showing only the same evolution of spectra that occurred for the mononuclear complexes, *viz.* collapse of the phenolate→$Mo^{V}$ LMCT transition and the appearance of a weak d–d transition associated with the molybdenum(IV) centres. No evidence for IVCT transitions in the reduced mixed-valence states was found except for $[\mathbf{1}]^{-}$ as detailed earlier.

### (vi) Molecular orbital calculations, and the nature of the oxidised forms of complexes 1–5 and 7–9

The intense, low-energy transitions of the oxidised forms of **1**–**5** could be consistent with the presence of a highly delocalised π system such as those found in extended quinones.[9–12] This agrees with our suggestion that ligand-centred oxidations could have occurred to give a dinuclear molybdenum(V) complex with a bridging neutral quinone in each case (Scheme 1), which was prompted by the electrochemical results. For example the delocalised π systems of nickel dithiolene complexes in some oxidation states give comparable near-IR transitions.[23] However two features of these spectra behaviour are inconsistent with this idea. First free di-,[10] ter-,[11] and tetra-phenobenzoquinones[12] have their π–π* absorptions at 394, 534 and 630 nm respectively, showing the expected drop in energy as the quinonoidal π systems lengthen: in contrast the absorption maxima of $[\mathbf{2}]^{2+}$–$[\mathbf{4}]^{2+}$ are essentially independent of the length of the bridging ligand. Secondly, the only free semiquinone radical anions of this type that have been spectroscopically characterised have their absorption maxima at much lower energy than that of the corresponding quinone.[10,24,25] For example, the absorption maximum of the *para*-biphenosemiquinone radical anion ($\lambda_{max}$ 800 nm, $\varepsilon$ 7500 $dm^3\ mol^{-1}\ cm^{-1}$) doubles in energy and becomes much more intense on further oxidation to *para*-biphenoquinone ($\lambda_{max}$ 394 nm, $\varepsilon$ 45 000 $dm^3\ mol^{-1}\ cm^{-1}$).[10] In contrast, oxidation of $[\mathbf{2}]^{+}$ to $[\mathbf{2}]^{2+}$ only causes the NIR transition to move from 1096 to 1017 nm with a much less significant change in intensity, and **3** and **4** show similar behaviour.

The alternative explanation for these strong NIR transitions is that, by analogy with the mononuclear complexes $[\mathbf{10}]^{+}$ and $[\mathbf{11}]^{+}$, and with the dinuclear complexes $[\mathbf{7}]^{2+}$–$[\mathbf{9}]^{2+}$ where a bridging quinone cannot be formed, they are phenolate-to-$Mo^{VI}$ LMCT processes, albeit at lower energy and having greater intensity than was seen for the mononuclear complexes. We saw earlier in $[\mathbf{10}]^{+}$ and $[\mathbf{11}]^{+}$ that an electron-donating substituent on the phenolate lowers the energy and raises the intensity of the LMCT bands, and the double negative charge on the bridging ligands of **1**–**5** means that each phenolate terminus effectively has a good electron-donor substituent (another phenolate anion) attached to it, which could account for the low energies of these bands. The much greater intensities of these bands for the dinuclear complexes compared to the mononuclear complexes can be ascribed partially (although not wholly) to the presence of two chromophores rather than one. In order to clarify the nature of these strong low-energy transitions we therefore performed molecular orbital calculations on some of these oxidised complexes (**10** as a representative mononuclear complex, and **2** as a representative dinuclear complex) using the ZINDO method.

To start with we performed calculations on the mononuclear complex **10** in its oxidised and reduced forms. In the molybdenum(VI) form $[\mathbf{10}]^{+}$ the HOMO is phenolate-based, and the LUMO is largely metal-based ($d_{xy}$), such that the lowest-energy transition is predicted to be phenolate→$Mo^{VI}$ LMCT. The calculated absorption maximum for this transition (690 nm) agrees very closely with what we observed (681 nm). The higher-energy transition in $[\mathbf{10}]^{+}$ at 475 nm also, as expected, has LMCT character, from the phenolate HOMO to the higher-energy metal d(π) orbitals ($d_{xz}$ and $d_{yz}$, which are close together). Its calculated wavelength of 430 nm agrees reasonably well with what we observed. In the reduced form $[\mathbf{10}]^{-}$ the low-lying d(*xy*) orbital is predicted to be doubly occupied giving a low-spin diamagnetic configuration, and the lowest-energy transition is predicted to be the weak d–d transition that we detected at about 800 nm (calculated, 1200 nm). In fact, because of the low concentrations used for the spectroelectrochemical experiments (in order to keep the strong π–π* transitions on-scale), we did not detect these weak d–d transitions in our first experiments, and only found them by repeating the reductions with more concentrated samples *after* the ZINDO calculations predicted that they should be present. In short the calculations on $[\mathbf{10}]^{+}$ and $[\mathbf{10}]^{-}$ show no surprises and the predicted electronic transitions are in good agreement with what we observed. Although the agreement between calculated and actual absolute energies for the electronic transitions is variable, qualitatively the number, nature and relative positions of the principal transitions are well accounted for.

Calculations on the oxidised dinuclear complex $[\mathbf{2}]^{2+}$ are complicated by the fact that the results depend on the bridging ligand conformation. At room temperature in solution a biphenyl spacer is expected to have free rotation about the central interannular C–C bond; the optimum dihedral angle, which minimises steric repulsion between the $H^2/H^6$ protons on adjacent rings yet still maintains as much conjugation in the π systems as possible, is about 32° in solution.[26] To gain some idea of the importance of bridging ligand conformation we performed the calculations under three conditions: (i) with the bridging ligand constrained to be planar; (ii) with the bridging ligand twisted at the intermediate angle of 32° which was predicted by a molecular mechanics energy minimisation using standard MM2 parameters and (iii) with the bridging

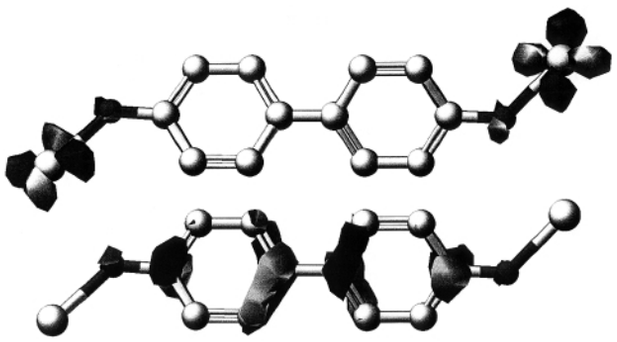

**Fig. 9** The HOMO (bottom) and LUMO (top) of complex $[2]^{2+}$ calculated by the ZINDO method. Only the metal ions and the bridging ligand are shown for clarity; the other atoms make no significant contribution to either orbital. A torsion angle of 32° between the phenyl rings has been assumed in this calculation (see text).

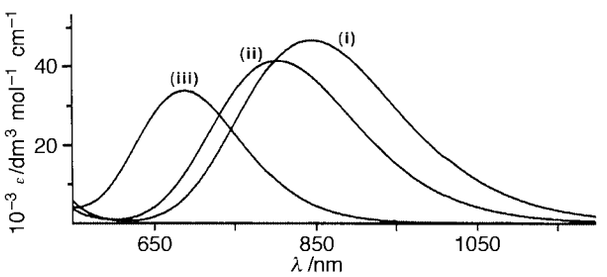


**Fig. 10** Predicted LMCT transitions in complex $[2]^{2+}$ from the ZINDO calculations, with twist angles of (i) 0, (ii) 32 and (iii) 90° between the two phenyl rings.

ligand constrained to have a 90° twist between the two phenyl rings.

Irrespective of bridging ligand conformation, the calculations showed that complex $[2]^{2+}$ is a $Mo^{VI}_2$ species, following metal-centred oxidation. The strong near-IR band is an LMCT transition from the HOMO, based on the bridging ligand, to the metal-centred degenerate pair of LUMOs (sum and difference combinations of the $d_{xy}$ orbitals on each metal); the orbitals involved are depicted in Fig. 9. The low energy of these transitions compared to those of the mononuclear molybdenum(VI) complexes arises because the bridging-ligand centred HOMO is relatively high in energy because of its double negative charge. As the bridging ligand is twisted the ZINDO calculations predict that the energy of this transition should increase and its intensity decrease, exactly as we observed by comparison of $[2]^{2+}$ and $[5]^{2+}$ (Fig. 10). Although the absolute energies of these transitions are somewhat overestimated by the ZINDO calculation (by *ca.* 20%), the *difference* that is calculated on changing the conformation of the bridging ligand agrees very well with what we observe. Thus the energy difference between the predicted absorption maxima with torsion angles of 32 ($\lambda_{calc} = 805$) and 90° ($\lambda_{calc} = 690$ nm) is 2070 $cm^{-1}$; the shift we actually observe between $[2]^{2+}$ ($\lambda_{obs} = 1017$) and $[5]^{2+}$ ($\lambda_{obs} = 832$ nm) is 2190 $cm^{-1}$. The low energies and high intensities of these near-IR transitions for $[2]^{2+}$–$[4]^{2+}$ compared to those of mononuclear $[10]^{+}$ are therefore consistent with the bridging ligands adopting conformations that are only moderately twisted, such that there is still substantial π overlap between the phenyl rings. Decoupling of the two termini would result in spectra closer to that observed for $[5]^{2+}$ with a 90° twist.

It appears therefore that the large redox separations between the two oxidations, which imply substantial delocalisation across the HOMO of the bridging ligand in the oxidised mixed-valence state, are facilitated by a near-planar conformation of the bridging ligand in the oxidised forms of the complex. It is tempting to suggest in turn that the very small redox separations between the reductions could arise because a more highly twisted conformation of the bridging ligand in the reduced mixed-valence state prevents delocalisation across it. This however does not account for the properties of **1** in which the bridging ligand is a single phenyl ring with no conformational flexibility, where the redox splitting between the oxidations is still much larger than it is between the reductions. The interplay of molecular orbital properties, redox properties and ligand conformations is clearly complex and is an interesting target for future, more sophisticated, computational studies.

### (vii) Comments on the intense near-IR transitions

The strong absorbance in the near-infrared region exhibited by the singly and doubly oxidised forms of many of these complexes is of special interest as such NIR dyes have a variety of potential applications. These include optical data storage devices, in which reading and writing of information is performed by diode lasers in the NIR region of the spectrum, Q-switching of lasers, whereby continuous low-energy output of such lasers in the NIR region is converted into very short, intense bursts, and photodynamic therapy, which takes advantage of the relative transparency of living tissue to NIR radiation.[27] If the NIR absorbance is not permanent but may be switched on by a redox change, then the material is electrochromic and of additional interest in the area of electro-optical switching if the absorbance maximum is close to the energy of the laser source used for optical information transfer.[14,15,28] We are currently attempting to exploit the properties of these complexes in some of these areas.

## Experimental

The complexes **1**–**6**,[4] **10**,[14] and $[Mo(Tp^{Me,Me})(O)Cl_2]$[6] were prepared according to the published methods. The ligands 4,4′-dihydroxydiphenylmethane (for **7**), 4,4′-thiodiphenol (for **8** and **8a**) and 4,4′-sulfonyldiphenol (for **9** and **9a**) were purchased from Aldrich and used as received.

Spectroelectrochemical measurements were performed at −30 °C in $CH_2Cl_2$, using a home-built OTTLE (optically transparent thin layer electrode) cell mounted in the sample compartment of a Perkin-Elmer Lambda 19 UV/VIS/NIR spectrometer; the details have been published elsewhere.[13] For all redox interconversions studied clean isosbestic points were observed except where explicitly stated otherwise, and the chemical reversibility of these processes was established by returning to the starting state and checking that the spectrum had not changed. ZINDO Calculations were performed on a CAChe workstation.[29]

### Preparations

Complexes **7**–**9** were prepared according to the usual method.[4] A mixture of the appropriate bridging ligand, 2.2 equivalents of $[Mo(Tp^{Me,Me})(O)Cl_2]$ and dry $Et_3N$ (0.5 $cm^3$, excess) was heated to reflux in dry toluene under $N_2$ for 8 h. After removal of the solvent *in vacuo* the solid residue was purified by column chromatography on silica using $CH_2Cl_2$ as eluent; the desired dinuclear complex was in every case the first intensely coloured band to elute. Following chromatographic isolation of **8** and **9**, their mononuclear analogues **8a** and **9a** were also isolated; these are slower-running fractions due to the polarity arising from their pendant hydroxyl groups. Yield and characterisation data are summarised in Table 1.

Complex **11** was prepared from a mixture of $[Mo(Tp^{Me,Me})(O)Cl_2]$ (0.20 g, 0.41 mmol) and 4-methoxyphenol (0.062 g, 0.50 mmol) in dry toluene (20 $cm^3$) containing dry $Et_3N$ (0.5 $cm^3$). The mixture was heated to 100 °C with stirring for 3 h under $N_2$ then cooled and the solvent removed *in vacuo*. The resulting solid was purified by column chromatography on silica gel using $CH_2Cl_2$–hexane (1 : 1, v/v), with the obvi-

**Table 6** Crystallographic data for complexes **8a** and **8**[a]

| | **8a** | **8**·$CH_2Cl_2$·0.5$C_6H_{14}$ |
|---|---|---|
| Formula | $C_{27}H_{31}BClMoN_6O_3S$ | $C_{46}H_{61}B_2Cl_4Mo_2N_{12}O_4S$ |
| $M$ | 661.84 | 1233.43 |
| System, space group | Monoclinic, $P2_1/c$ | Triclinic, $P\bar{1}$ |
| $a$/Å | 13.581(2) | 10.8807(12) |
| $b$/Å | 17.475(3) | 15.5555(13) |
| $c$/Å | 12.663(1) | 16.969(3) |
| $\alpha$/° | | 80.708(10) |
| $\beta$/° | 104.772(7) | 79.243(14) |
| $\gamma$/° | | 76.397(7) |
| $U$/Å$^3$ | 2905.9(7) | 2721.7(6) |
| $Z$ | 4 | 2 |
| $D_c$/g cm$^{-3}$ | 1.513 | 1.505 |
| $\mu$/mm$^{-1}$ | 0.655 | 0.749 |
| Crystal size/mm | 0.45 × 0.2 × 0.2 | 0.4 × 0.3 × 0.3 |
| Reflections collected: total, independent, $R_{int}$ | 29491, 6675, 0.0254 | 28471, 12324, 0.0323 |
| Data, restraints, parameters | 6675, 0, 390 | 12321, 3, 696 |
| Final $R1$, $wR2$[a] | 0.0459, 0.1043 | 0.0507, 0.1648 |
| Largest residuals/e Å$^{-3}$ | +0.571, −1.008 | +0.784, −1.511 |

[a] Structure was refined on $F_o^2$ using all data; the values of $R1$ is given for comparison with older refinements based on $F_o$ with a typical threshold of $F \geqslant 4\sigma(F)$.

ous principal dark coloured fraction being collected in each case. Yield and characterisation data are summarised in Table 1.

### X-Ray crystallography

Crystals of complexes **8a** and **8**·$CH_2Cl_2$·0.5$C_6H_{14}$ were grown by slow diffusion of hexane in to concentrated $CH_2Cl_2$ solutions of the complexes. Suitable crystals were mounted on a Siemens SMART diffractometer in a stream of cold $N_2$ at −100 °C. A detailed experimental description of the methods used for data collection and integration using the SMART system has been published.[30] Data were collected to $2\theta_{max} = 55°$ at −100 °C using graphite-monochromatised Mo-Kα X-radiation ($\lambda$ 0.71073 Å), and after integration of the data and merging of equivalent reflections were absorption-corrected using SADABS.[31] Details of the crystal parameters, data collection and refinement are summarised in Table 6. The structures were solved by conventional or direct methods, and refined by the full-matrix least-squares method using all $F^2$ data, using the SHELX suite of programs.[32] All non-hydrogen atoms were refined with anisotropic thermal parameters; hydrogen atoms were included in calculated positions and refined with isotropic thermal parameters riding on those of the parent atom.

In both structures disorder between the oxo and chloride ligands attached to each metal site was observed. For complex **8a** these atoms were refined with site occupancies of 50% for the two components. For **8**·$CH_2Cl_2$·0.5$C_6H_{14}$ the extent of disorder appeared to be slightly different at Mo(1) and Mo(2). Thus O(1) and Cl(1) [attached to Mo(1)] were refined with site occupancies of 44 and 56% for their two orientations; for O(2) and Cl(2) [attached to Mo(2)] the site occupancies were 59 and 41%. The unit cell of this structure also contains a hexane molecule astride an inversion centre, such that three carbon atoms are present in the asymmetric unit.

CCDC reference number 186/1491.

See http://www.rsc.org/suppdata/dt/1999/2417/ for crystallogrpahic files in .cif format.

## Acknowledgements

The following agencies are thanked for financial support: EPSRC (UK), the Croucher foundation (Hong Kong), and the European Community TMR Network programme (contract no. EC-CHRX-CT96-0047).

## References

1 J. A. McCleverty and M. D. Ward, *Acc. Chem. Res.*, 1998, **31**, 842.
2 M. D. Ward, *Chem. Soc. Rev.*, 1995, 121; *Chem. Ind.* (*London*), 1996, 568.
3 Some representative recent examples: J.-M. Tour, M. Kozaki and J. M. Seminario, *J. Am. Chem. Soc.*, 1998, **120**, 8486; S. Anderson, R. T. Aplin, T. D. W. Claridge, T. Goodson, A. C. Maciel, G. Rumbles, J. F. Ryan and H. L. Anderson, *J. Chem. Soc.*, *Perkin Trans. 1*, 1998, 2383; A. P. H. J. Schenning, R. E. Martin, M. Ito, F. Diederich, C. Boudon, J.-P. Gisselbrecht and M. Gross, *Chem. Commun.*, 1998, 1013; A. Harriman and R. Ziessel, *Coord. Chem. Rev.*, 1998, **171**, 331; I. Jestin, P. Frere, P. Blanchard and J. Roncali, *Angew. Chem.*, *Int. Ed. Engl.*, 1998, **37**, 942; R. D. Adams, T. Barnard, A. Rawlett and J.-M. Tour, *Eur. J. Inorg. Chem.*, 1998, 429; S. N. Yaliraki and M. A. Ratner, *J. Chem. Phys.*, 1998, **109**, 5036; B. W. Jiang, S. W. Yang, S. L. Bailey, L. G. Hermans, R. A. Niver, M. A. Bolcar and W. E. Jones, *Coord. Chem. Rev.*, 1998, **171**, 365; L. Jaquinod, O. Siri, R. G. Khoury and K. M. Smith, *Chem. Commun.*, 1998, 1261.
4 V. A. Ung, D. A. Bardwell, J. C. Jeffery, J. P. Maher, J. A. McCleverty, M. D. Ward and A. Williamson, *Inorg. Chem.*, 1996, **35**, 5290.
5 V. A. Ung, A. M. W. Cargill Thompson, D. A. Bardwell, D. Gatteschi, J. C. Jeffery, J. A. McCleverty, F. Totti and M. D. Ward, *Inorg. Chem.*, 1997, **36**, 3447.
6 W. E. Cleland, Jr., K. M. Barhhart, K. Yamanouchi, D. Collison, F. E. Mabbs, R. B. Ortega and J. H. Enemark, *Inorg. Chem.*, 1987, **26**, 1017.
7 W. Bruns, W. Kaim, E. Waldhör and M. Krejcik, *Inorg. Chem.*, 1995, **34**, 663; M. Ketterle, J. Fiedler and W. Kaim, *Chem. Commun.*, 1998, 1701.
8 A. Wlodarczyk, G. A. Doyle, J. P. Maher, J. A. McCleverty and M. D. Ward, *Chem. Commun.*, 1997, 769.
9 K. Takahashi, A. Gunji, K. Yamagi and M. Miki, *J. Org. Chem.*, 1996, **61**, 4784; K. Takahashi, T. Suzuki, K. Akiyama, Y. Ikegami and Y. Fukazawa, *J. Am. Chem. Soc.*, 1991, **113**, 4576.
10 W. J. Detroit and H. Hart, *J. Am. Chem. Soc.*, 1952, **74**, 5215; O. B. Lantratova, A. I. Prokof'ev, I. V. Khudyakov, V. A. Kuzmin and I. F. Pokrovskaya, *Nouv. J. Chim.*, 1982, **6**, 365.
11 R. West, J. A. Jorgensen, K. L. Stearley and J. C. Calabrese, *J. Chem. Soc.*, *Chem. Commun.*, 1991, 1234; P. Boldt, D. Bruhnke, F. Gerson, M. Scholz, P. G. Jones and F. Bär, *Helv. Chim. Acta*, 1993, **76**, 1739.
12 A. Rebmann, J. Zhou, P. Schuler, H. B. Stegmann and A. Rieker, *J. Chem. Res.* (*M*), 1996, 1765.
13 S.-M. Lee, R. Kowallick, M. Marcaccio, J. A. McCleverty and M. D. Ward, *J. Chem. Soc.*, *Dalton Trans.*, 1998, 3443.
14 S.-M. Lee, M. Marcaccio, J. A. McCleverty and M. D. Ward, *Chem. Mater.*, 1998, **10**, 3272.
15 A. M. Barthram, R. L. Cleary, R. Kowallick and M. D. Ward, *Chem. Commun.*, 1998, 2695.

16 A. M. Barthram, R. L. Cleary, J. C. Jeffery, S. M. Couchman and M. D. Ward, *Inorg. Chim. Acta*, 1998, **267**, 1; L. F. Joulié, E. Schatz, M. D. Ward, F. Weber and L. J. Yellowlees, *J. Chem. Soc.*, *Dalton Trans.*, 1994, 799.
17 T. E. Keyes, R. J. Forster, P. M. Jayaweera, C. G. Coates, J. J. McGarvey and J. G. Vos, *Inorg. Chem.*, 1998, **37**, 5925.
18 V. A. Ung, S. M. Couchman, J. C. Jeffery, J. A. McCleverty, M. D. Ward, F. Totti and D. Gatteschi, *Inorg. Chem.*, 1999, **38**, 365.
19 S. M. Charsley, C. J. Jones, J. A. McCleverty, B. D. Neaves and S. J. Reynolds, *J. Chem. Soc.*, *Dalton Trans.*, 1998, 301.
20 H. Fischer, G. Tom and H. Taube, *J. Am. Chem. Soc.*, 1976, **98**, 5512.
21 I. de S. Moreira and D. W. Franco, *Inorg. Chem.*, 1994, **33**, 1607; *J. Chem. Soc.*, *Chem. Commun.*, 1992, 450.
22 D. A. Bardwell, D. Black, J. C. Jeffery, E. Schatz and M. D. Ward, *J. Chem. Soc.*, *Dalton Trans.*, 1993, 2321; G. K. Lahiri, S. Bhattacharya, B. K. Ghosh and A. Chakravorty, *Inorg. Chem.*, 1987, **26**, 4324.
23 U. T. Mueller-Westerhof, B. Vance and D. I. Yoon, *Tetrahedron*, 1991, **47**, 909; F. Bigoli, P. Deplano, M. L. Mercuri, M. A. Pellinghelli, G. Pintus, E. F. Trogu, G. Zonnedda, H. H. Wang and J. M. Williams, *Inorg. Chim. Acta*, 1998, **273**, 175; H. Shiozaki, H. Kakazumi, Y. Nakado and T. Kitao, *Chem. Lett.*, 1987, 2393; J. A. McCleverty, *Prog. Inorg. Chem.*, 1968, 1049.
24 J. Mayer and R. Krasiunkianis, *J. Chem. Soc.*, *Faraday Trans.*, 1991, 2943; P. S. Rao and E. Hayon, *J. Phys. Chem.*, 1973, **77**, 2274; R. H. Schuler, G. N. R. Tripathi, M. F. Prebenda and D. M. Chipman, *J. Phys. Chem.*, 1983, **87**, 5357.
25 E. A. Braude, *J. Chem. Soc.*, 1945, 490; A. Kuboyama, S. Matsuzaki, H. Takagi and H. Arano, *Bull. Chem. Soc. Jpn.*, 1974, **47**, 1604.
26 V. J. Eaton and D. Steele, *J. Chem. Soc.*, *Faraday Trans. 2*, 1973, 1601.
27 M. Emmelius, G. Pawlowski and H. W. Vollmann, *Angew. Chem.*, *Int. Ed. Engl.*, 1989, **28**, 1445; J. Fabian and R. Zahradnik, *Angew. Chem.*, *Int. Ed. Engl.*, 1989, **28**, 677; J. Fabian, H. Nakazumi and M. Matsuoka, *Chem. Rev.*, 1992, **92**, 1197.
28 M. D. Ward, *Chem. Ind.*, 1997, 640; K. Yoshida, N. Oga, M. Kadota, Y. Ogasahara and Y. Kubo, *J. Chem. Soc.*, *Chem. Commun.*, 1992, 1114; Y. Kubo, *J. Chem. Soc.*, *Perkin Trans. 1*, 1994, 2521.
29 ZINDO version 4.0.2 in the CAChe system, Oxford Molecular, Oxford, 1998.
30 P. L. Jones, A. J. Amoroso, J. C. Jeffery, J. A. McCleverty, E. Psillakis, L. H. Rees and M. D. Ward, *Inorg. Chem.*, 1997, **36**, 10.
31 SADABS, A program for absorption corrections using the Siemens SMART diffractometer system, G. M. Sheldrick, University of Göttingen, 1996.
32 SHELXTL 5.03 program system, Siemens Analytical X-Ray Instruments, Madison, WI, 1995.

*Paper 9/03841H*